Research Article | Vol. 31, No. 2 / 16 Jan 2023 / Optics Express 2234
Optics EXPRESS

Ultra-precision manufacturing of microlens arrays using an optimum machining process chain

SHIXIANG WANG,[1,2] LINGBAO KONG,[1,3,*] CHUNJING WANG,[2] AND CHIFAI CHEUNG[2,4]

[1]*Shanghai Engineering Research Center of Ultra-Precision Optical Manufacturing, School of Information Science and Technology, Fudan University, Shanghai, China*
[2]*State Key Laboratory of Ultra-Precision Machining Technology, Department of Industrial and Systems Engineering, The Hong Kong Polytechnic University, Hung Hom, Kowloon, Hong Kong*
[3]*Yiwu Research Institute, Fudan University, Chengbei Road, Yiwu City 322000, China*
[4]*Benny.Cheung@polyu.edu.hk*
[*]*LKong@fudan.edu.cn*

Abstract: There are still significant challenges in the accurate and uniform manufacturing of microlens arrays (MLAs) with advanced ultra-precision diamond cutting technologies due to increasingly stringent requirements and shape complexity. In this paper, an optimum machining process chain is proposed based on the integration of a micro-abrasive fluid jet polishing (MAFJP) process to improve the machining quality by single point diamond turning (SPDT). The MLAs were first machined and compensated by SPDT until the maximum possible surface quality was obtained. The MAFJP was used to correct the surface form error and reduce the nonuniformity for each lens. The polishing characterization was analyzed based on the computational fluid dynamics (CFD) method to enhance the polishing efficiency. To better polish the freeform surface, two-step tool path generation using a regional adaptive path and a raster and cross path was employed. Moreover, the compensation error map was also investigated by revealing the relationship between the material removal mechanism and the surface curvature and polishing parameters. A series of experiments were conducted to prove the reliability and capability of the proposed method. The results indicate that the two integrated machining processes are capable of improving the surface form accuracy with a decrease in *PV* value from 1.67 μm to 0.56 μm and also elimination of the nonuniform surface error for the lenses.

1. Introduction

Microlens arrays (MLAs) have been widely used in many advanced imaging and illuminating systems due to their excellent optical properties, such as highly efficient light transmission [1,2] and small laser beam spot size [3]. These MLAs are usually classified as a type of structure freeform surface. The increasing shape complexity and high surface quality demanded for difficult-to-machine materials for optics imposes new challenges for manufacturing products with high efficiency and high accuracy. Various machining techniques have been developed, such as chemical wet etching [4] and electrical discharge machining [5]. These methods are mostly used for mass production of microlens arrays fabrication and not only require the use of relatively expensive equipment but can also lead to disadvantages of low uniform surface quality. Moreover, it has been reported that these etching processes can pose a public health and environmental risk because of the poisonous chemicals used [6]. Compared with nonmechanical methods, micromilling, laser-assisted machining and ultra-precision machining techniques also provide a more flexible way to manufacture these optics. Among these techniques, ultra-precision techniques using a single diamond machining method are dominant and are expected to be one

#479696 https://doi.org/10.1364/OE.479696
Journal © 2023 Received 3 Nov 2022; revised 23 Nov 2022; accepted 28 Nov 2022; published 9 Jan 2023

Optics EXPRESS

of the most promising ways to generate freeform surfaces with sub-micro form accuracy and a nanoscale surface finish [7].

In advanced ultra-precision diamond machining methods, three types of machining MLAs methods are well known, including the fast tool servo, slow tool servo and milling [8,9]. Li et al. [10] proposed 3-axis ultra-precision machining of MLAs assisted by a developed on-machine measurement system. A 2×2 microlens array was successfully machined, and its surface quality was found to be improved by an average of more than 40%. One challenge for these methods is that the developed on-machine measurement system needs to be well calibrated and the motion error also needs to be separated. Mukaida et al. [11] proposed a tool-servo driven segment turning method to reduce the dynamic error of the machine tool induced by lenslet edges during lens array cutting. A termed toroid-surface-based slow tool servo turning method was developed for generation of discontinuously structured microlens arrays in [12]. Sun et al. [13] developed a self-tuned diamond milling system for fabricating infrared micro-optics arrays with improved surface uniformity and machining efficiency. Optical elements on single-crystal silicon with a form error of 60 nm were successfully fabricated. Additionally, Kim et al. [14] also proposed a tilted milling method to eliminate the tool error on a 5-axis ultra-precision diamond machine. The form accuracy of the MLAs was found to be sharply improved by tilting the tool-axis angle by 35°. Although these novel enhanced diamond machining methods have achieved great success, they are restricted to limited features of MLAs on specified materials or machine tools.

In recent years, a micro-abrasive fluid jet polishing (MAFJP) was increasing employed for manufacturing freeform optics, which involves polishing the surface with a premixed slurry (water and micro-abrasive particles) at low pressures. MAFJP has the advantages of no heat generation and no tool wear, high machining accuracy with a nanoscale material removal rate, and suitability for various materials [15]. Most researchers in this field have paid attention to material removal theory or machining parameter optimization [16]. The application of machining MLAs has received little attention. Wang et al. [17] developed a fluid jet-array parallel machining method to improve the productivity and uniformity of MLAs. Furthermore, they also investigated the performance of a maskless fluid jet polishing method on a sinusoidal structured surface and V-groove structured surface [18]. However, the proposed methods are still limited by their low machining efficiency and low surface quality for a glass surface.

As a result, in this paper, a novel fabrication method that combined the advantages of single diamond turning and micro-abrasive fluid jet polishing to reduce the nonuniformity and improve the surface quality of manufactured MLAs is proposed. In Section 2, the framework for the proposed method is described, and the main machining parameters affecting the error correction are also analyzed. In the following sections, a series of experiments on 3×3 MLAs are conducted to validate the process chain, and the results are then discussed.

2. Methodology

2.1. Integrated machining process chain for manufacturing MLAs

The schematic of the integrated machining process chain for manufacturing MLAs is illustrated in Fig. 1. According to the requirement of the surface feature, the designed MLAs were first machined using the ultra-precision machine tool with optimized machining parameters and proper tool path generation. The machined surface was then measured in a high-precision 3D optical instrument. After determining the surface error, a compensation process is indispensable if the surface quality is far from that required. In this process, a re-clamping operation can introduce new errors, and even a small positioning error can lead to a severe deviation in the surface form. To minimize this kind of error, a positioning method using references and an additional measuring instrument was used. When several cycles of the SPDT were conducted and the surface quality was still out of requirement, the second process chain MAFJP was carried out. Similar to the SPDT process, the surface form error for the MLAs was first transformed to

Optics EXPRESS

the polishing system through the positioning process, and then a two-step polishing tool path plan was generated with well-selected parameters. If the surface error was still larger than the specification, corrective polishing cycles with optimized parameters were used.

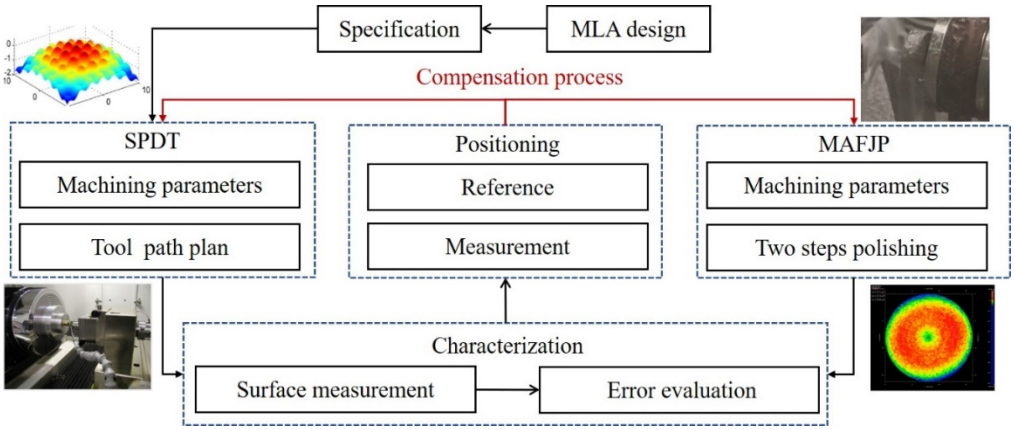

Fig. 1. Schematic of the combined process chain for manufacturing the MLAs.

2.2. Ultra-precision machining of MLAs by the SPDT process

SPDT is a reliable and robust process for manufacturing microstructures on many materials with high form accuracy and low surface roughness. As shown in Fig. 2, the manufacturing process starts from the structural design of the MLAs. Based on the material and surface geometry, analysis was performed to determine the optimum tool radius, cutting depth. The tool path was then determined based on the geometry of the surface. In this process, a modified tool path was applied to minimize the deviation between the machined surface and the designed surface.

2.3. Positioning method

Because the evaluated errors for the surface need to be transformed accurately as much as possible from the measuring coordinate system to the jet polishing coordinate system, it is important to position the locations of the lenses in the polishing system. Considering that the evaluated errors are embedded in the design coordinate system of the surface, a possible solution that can reduce the positioning errors was proposed. As shown in Fig. 3, a fixture with two perpendicular planes was designed with consideration of characterizations of the machine tools and workpieces. The workpiece was then mounted on the fixture and the MLA surface was treated as the plane and it is perpendicular to the other two planes. Hence, three mutually perpendicular planes processed by ultra-precision machining were used as reference surfaces, and the machined errors for these surfaces were lower than 0.2 µm in terms of the *PV* value. Hence, the surface H and surface V can guarantee the consistency of the *xoz* and *x'o'z'*, *yoz* and *y'o'z'* planes in the design coordinate and polishing coordinate system, respectively. Surface W can ensure that the *xoy* and *x'o'y* planes are parallel. However, the target machined surface W can be scratched by the touch probe (Mahr Federal Inc), although it only generates a small force, as shown in Fig. 3(b). According to simulated results in Fig. 6, material removal is less sensitive to the distance in the *z* direction; therefore, only three noncollinear points around the edge of the workpiece were selected for measurements.

Optics EXPRESS

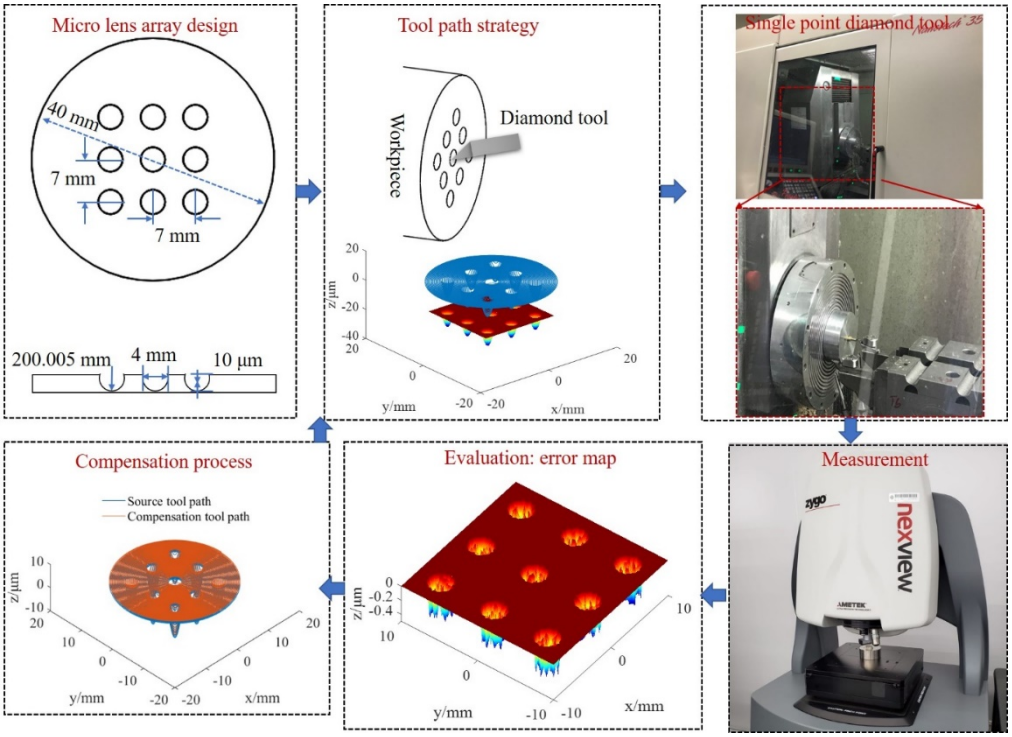

Fig. 2. Process chain for fabrication of MLAs using an ultra-precision machine tool.

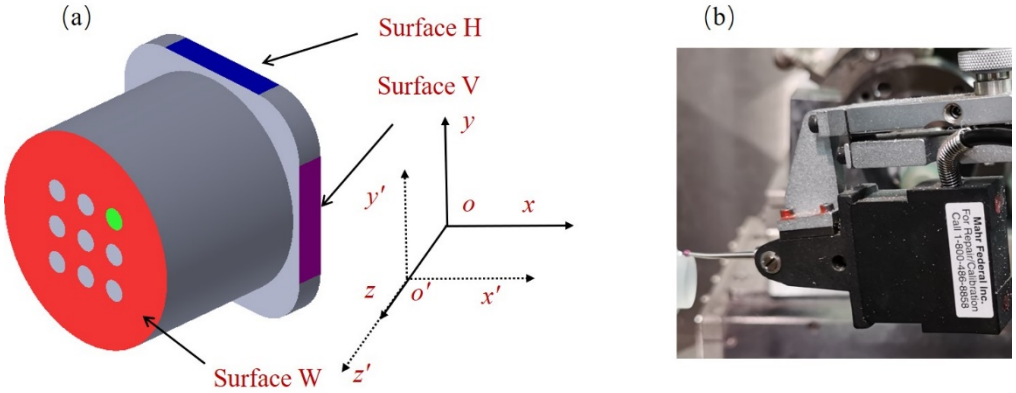

Fig. 3. Positioning strategy: (a) Processed surface for positioning the workpiece, (b) measurement device.

2.4. Surface improvement by micro-abrasive fluid jet polishing

Following the positioning process, the MAFJP process was employed to further improve the surface quality. In the proposed method, the key technique to ensure the surface quality is the micro-abrasive fluid jet polishing process. It is necessary to determine the main parameters that influence the accuracy and efficiency in the polishing cycle. Figure 4 presents the experimental setup used, a 7-axis polishing machine, and shows a schematic illustration of the MAFJP. The slurry consists of water and micro-abrasives contained in a tank that can be pumped at a certain

Optics EXPRESS

pressure to the nozzle. The stand-off distance, impingement angle and other parameters are considered to have a great influence on the material removal.

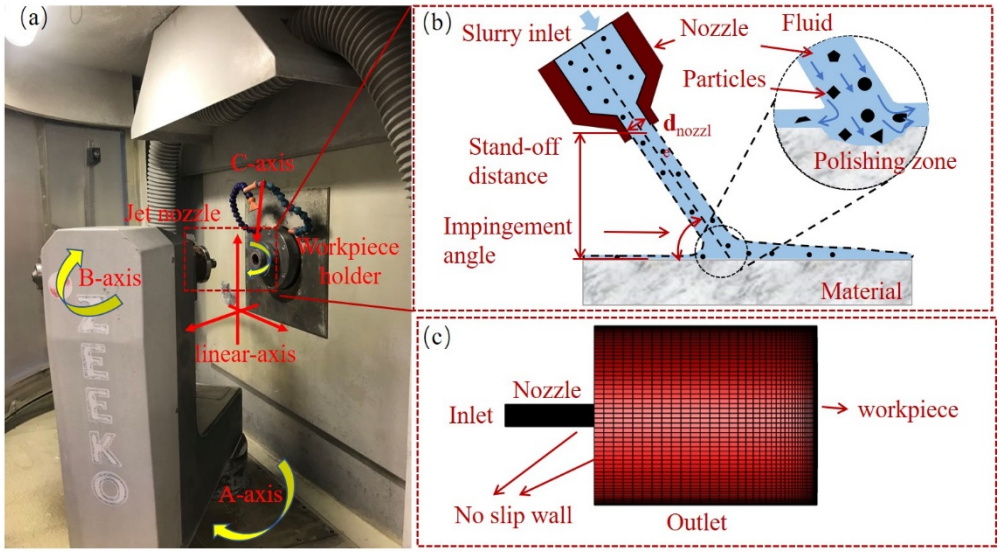

Fig. 4. (a) 7-axis polishing machine tool, (b) schematic illustration of abrasive water jet polishing, and (c) simulation model in FLUENT.

To better understand the material removal mechanism for the MAFJP process, several groups of simulations were conducted using a computational fluid dynamics (CFD) model packaged in FLUENT software, which has been previously proven to be reliable by many researchers for providing deep insights into multiphase flow systems [19–22]. The diameter of the nozzle d_{nozzle} was 0.5 mm. Al6061 was used as the workpiece material and 10 wt.% 4000# silicon carbide was used as the slurry. The average size of the abrasive particles was 3.2 µm. It is assumed that the fluid flow shows the properties of incompressibility and constant density. A volume of fluid (VOF) model was selected based on the Navier–Stokes equation to solve for the multiphase solution. A shear stress transport (SST) *k-w* model was used to describe the turbulence on the flow [20]. The simulation results are also based on the boundary conditions defined in Fig. 4.

Figure 5 shows the simulated tool influence function at a certain condition. The TIF shape of the MAFJP can be described by a type of Gaussian radial distribution. It is common to describe the Gaussian shape removal function as follows:

$$R(x, y) = Pexp[-B \cdot (x^2 + y^2)] \tag{1}$$

where P is the coefficient related to the peak value, and B is the coefficient of the Gaussian shape. Related publications [23] have reported the P and B values for various material and polishing conditions; however, there is still no unified and exact model for describing the specific polishing process. To accurately express our task-specific polishing process, the simulated digital material removal at a unit time was employed to present the TIF.

In addition, polishing conditions that can influence the TIF are also discussed. Table 1 shows the designed polishing conditions in the experiments. Figure 6 shows the material removal rate (MRR) for all the sample groups. For easy observation, the MRR is normalized over a range of 0 to 1 mm^3/min.

According to the simulated results, the stand-off distance (SOD) has a limited effect on the MRR compared with the pressure and dwell time. A higher pressure and a longer polishing time

Optics EXPRESS

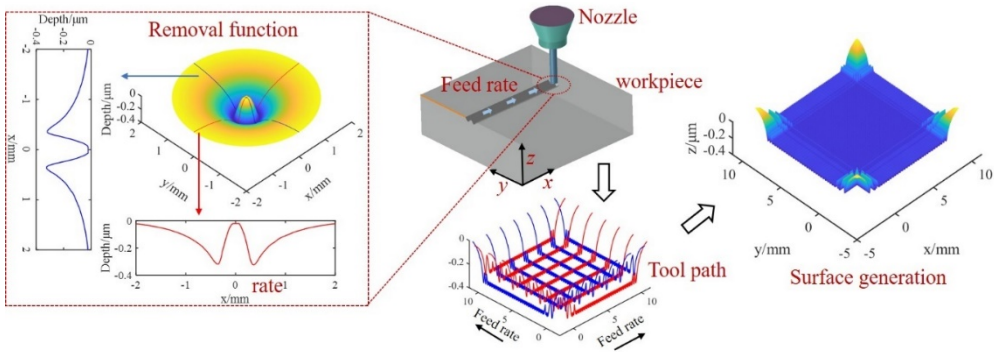

Fig. 5. Tool influence function and the corresponding surface generation using a raster and cross polishing tool path.

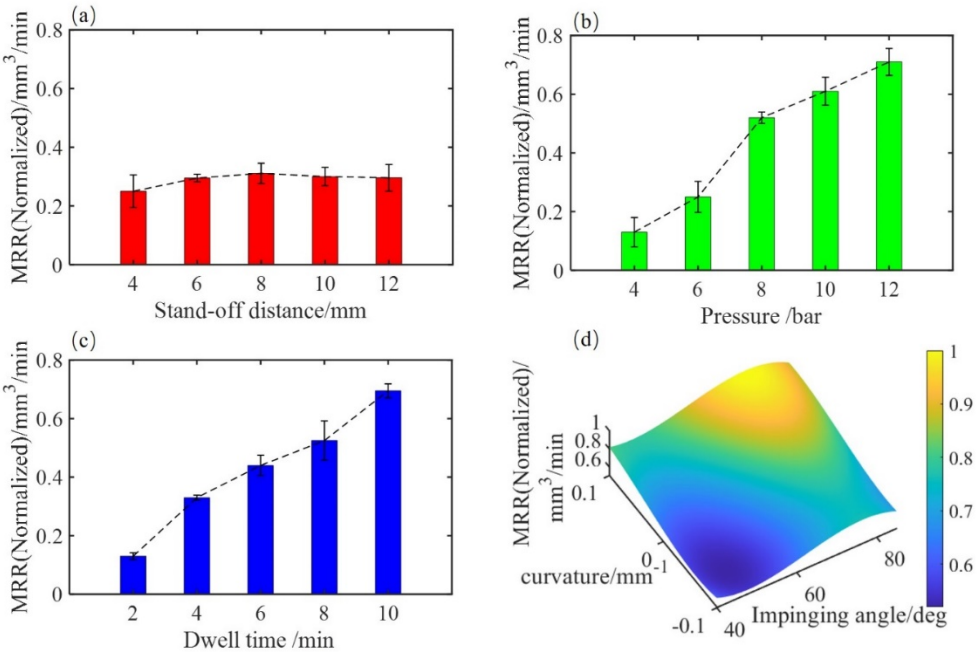

Fig. 6. Factors that influence the TIF: (a) different stand-off distances, (b) different fluid pressures, (c) different dwell times, and (d) a fitted model of the MRR varying with the different surface curvatures and impinging angles.

Table 1. Polishing conditions designed for analyzing the material removal rate

Conditions	Group 1	Group 2	Group 2	Group 4
Stand-off distance (mm)	4,6,8,10,12	8	8	8
Pressure (bar)	8	4,6,8,10,12	8	8
Dwell time	6	6	2,4,6,8,10	6
Impingement angle (deg)	90	90	90	40,50,60,70,80,90
Radius of curvature (mm)	∞	∞	∞	10,20. . . 100; ∞ -10, -20, . . . -100

Optics EXPRESS

can lead to enhanced material removal. The surface curvature and impingement angle show a slight effect on the MRR, which can be summarized by a similar relationship to that reported in Ref. [24] as follows:

$$f(\theta, c) = \alpha_1 + \alpha_2\theta + \alpha_3 c + \alpha_4\theta^2 + \alpha_5 c^2 + \alpha_6\theta c + \alpha_7\theta^3 + \alpha_8 c^3 + \alpha_9\theta^2 c + \alpha_{10}\theta c^2 \quad (2)$$

where α are the coefficients of the polynomials and θ and c denote the impingement angle and curvature, respectively. It is noted that this fitted model can be used to compensate for the freeform surface polishing process, especially when the form errors are distributed nonuniformly.

Tool path generation is an important step in the fabrication of freeform optics or MLAs with high accuracy and efficiency. Various polishing tool paths have been explored for optical surface generation. Tam et al. [25] compared four common paths, the bi-scanning path, spiral path, Hilbert path and Peano path, theoretically and experimentally. Beaucamp et al. [26] also developed a circular-random path to reduce mid-spatial frequency errors freeform optics. Well-distributed changes in the tool path direction and well-balanced direction of the path lines can improve the uniformity of the polishing. Based on this conclusion, Cao et al. [27] proposed a new method that combined raster and cross polishing tool paths on both difficult-to-machine materials and ductile materials. The results proved that this method can be used to polish the freeform surface. Considering the characterization of the MLAs, the same theoretical modeling of the surface generation was used as one part of the tool path plan in our research, and the simulation result is shown in Fig. 5. It can also be observed that the theoretical form error for the flat workpiece with dimensions of 10 mm × 10 mm ranges from 0 to 0.4 μm.

However, in our case, the regions with relatively large form errors need to be polished too, especially those regions around each lens. Apart from the raster and cross polishing tool path, another adaptive tool path method must be developed so that the paths only pass through the areas of interest. Inspired by Ref. [28], a hexagonal meshing-based adaptive polishing method is proposed so that the nonuniform sampling points on the surface can be used to generate the tool path. If the error for the center of the hexagonal cell is present in the regions, the cell can be treated as a reachable part. As illustrated in Fig. 7, the whole surface needs to be polished using a two-step process. In step one, the error map for the MLA surface is generated (Fig. 7(a)), and then the mainly focused-on processing regions (Fig. 7(b)) for each lens can be determined using Eq. (3):

$$\begin{aligned} Rgs &= \{(x, y) | error(x, y) \rangle thr\} \\ error &= error_m + 2RMS_{surface} \\ thr &= RMS_{central} > \lambda/20 \end{aligned} \quad (3)$$

where $error_m(x,y)$ is the evaluated error map, thr is the given threshold, which is determined by the RMS value of the central lens (RMS_{central}) and should be larger than $\lambda/20$ because the form error of most optical surfaces should be less than this value. The error map $error$ (x,y) of interest is then determined by increasing the RMS value for the surface ($RMS_{surface}$) by two times. Rgs denotes the regions of interest on the surface.

The processing regions are then represented by hexagonal grids (Fig. 7(c)). Hence, the polishing path can move along the boundaries of the adjacent hexagons, as shown in Fig. 7(d).

To improve the smoothness and stability of the polishing process, some outliers are removed, and the path is also filtered by a selected Gaussian function. Conventionally, the material removal rate can be modeled by the assumption that the TIF moves along a specific tool path at a constant velocity. In general, the total amount of material removal can be determined by convoluting the

Optics EXPRESS

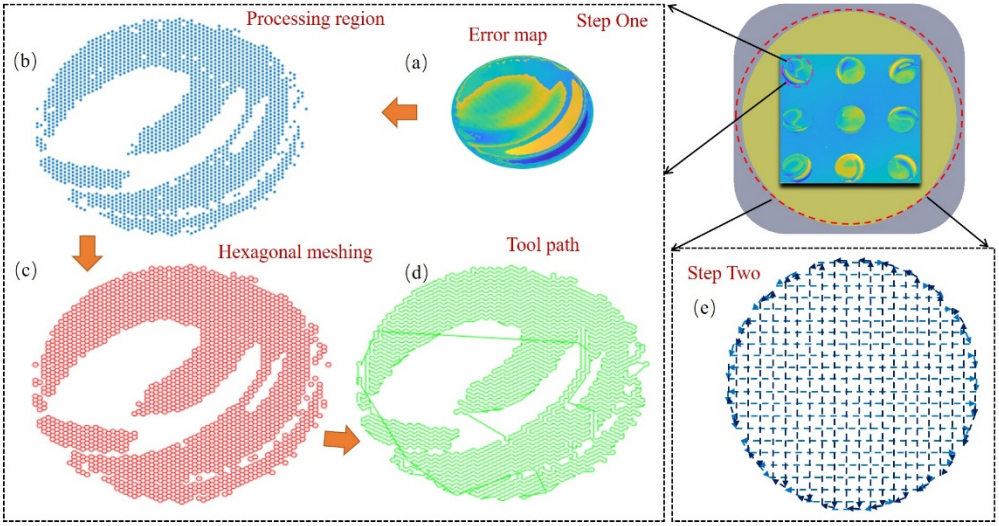

Fig. 7. Two-step tool path generation method. (a) Error map for the lens, (b) Processing region with a large form error, (c) Hexagonal meshing of the error areas, (d) Tool path generation along the boundaries of the hexagonal cells, (e) Combined raster and cross polishing tool path.

TIF and the dwell time map along the tool path, which can be expressed as follows [24]:

$$\begin{aligned} MR(x,y) &= R(x,y) * T(x,y) \\ &= \iint_{\text{path}} R(x-x', y-y') \cdot T(x-x', y-y')\, dx'dy' \end{aligned} \tag{4}$$

where MR is the material removal on the surface, $R(x, y)$ and $T(x, y)$ denote the TIF and corresponding dwell time function, respectively, and $(x - x', y - y')$ is the transformation relationship between the TIF and polishing system.

If the initial surface form $MR_0(x, y)$ is given, it is easy to see that the polished freeform surface can be generated by

$$f(x,y) = MR_0(x,y) - MR(x,y) \tag{5}$$

In our case, the material removal can be different due to the nonuniform sampling points obtained using Eq. (4). To precisely describe the material removal, a modified linear equation is employed:

$$\widetilde{MR}(x,y) = \tilde{R}(x,y) \cdot \tilde{T}(x,y) \tag{6}$$

where $\widetilde{MR}(x, y)$ is a column vector obtained by reshaping, $MR(x, y)$, and $\tilde{T}(x, y)$ is also a column vector that contains the dwell time for each sampling point. $\tilde{R}(x, y)$ is a transformation matrix that contains TIFs. As a result, the dwell time can be calculated using the following equation:

$$minE(\tilde{T}) = min\{\Delta|\widetilde{error}(x,y) - \tilde{R}(x,y) \cdot \tilde{T}(x,y)\} \tag{7}$$

This equation can be solved by introducing an exponential penalty function, as presented in Refs. [28,29]. Following the step one polishing process, the raster and cross polishing tool path, as shown in Fig. 7(e), is carried out to remove the tool mark of the previous polishing process and further improve the surface quality.

Optics EXPRESS

3. Experimental study

3.1. Ultra-precision single point diamond turning process

To validate the proposed process chain for improving the surface quality, three groups of 3×3 MLAs composed of aluminum alloy were first manufactured by a single-point diamond turning machine (Moore Nanotech 450 UPL). For a 3×3 MLA, the curvature radius and chord height of a single lens-let are 200.005 mm and 10 µm, respectively. Other parameters are listed in Table 2. The machining experiments were conducted using a 4-axis ultra-precision machine with the slow tool servo technique, and the machining parameters are listed in Table 3. A spiral path was applied for tool path generation. After the machining process, the profile of the machined MLAs was measured with a white light interferometer (Zygo Nexview, 10X). Considering the inevitable errors generated by tool vibration or other systematic error, one to two compensation processes are required for the MLAs after surface evaluation.

Table 2. MLA design parameters

Sample material	Aluminum 6061
Pattern	3×3
Nominal shape	Sphere
Spacing	7 mm
Aperture radius	4 mm
Chord height	10 µm
Radius of curvature	200.005 mm

Table 3. Processing parameters for slow tool servo machining of MLAs

Tool tip radius	0.514 mm
Rake angle	0 deg
Clearance angle	10 deg
Included angle	60 deg
Spindle speed	50 rpm
Feed rate	10 mm/min
Cutting depth	2 µm

3.2. MLAs characterization

To achieve a better surface quality for the MLAs, two cycles of the process chain mentioned above were performed. An iterative closest point (ICP) registration algorithm [30] was used for matching two distinct surfaces. However, the ICP algorithm is sensitive to the initial given parameters and can be trapped in a local minimum. The registration process may affect the final surface residual error. Taking the surface features of MLAs into consideration, the local lowest points for the nine lenses were used to limit the initial parameters. One of the machined workpieces and its 3D error map are shown in Fig. 8.

The form errors for the holistic surface range from -1.66 µm to 1.49 µm without the removal of some outliers. Two parameters, the root mean square (*RMS*) and peak-to-valley (*PV*) values, defined by Eq. (8) were widely used to characterize the surface quality of the MLA surface. The

Optics EXPRESS

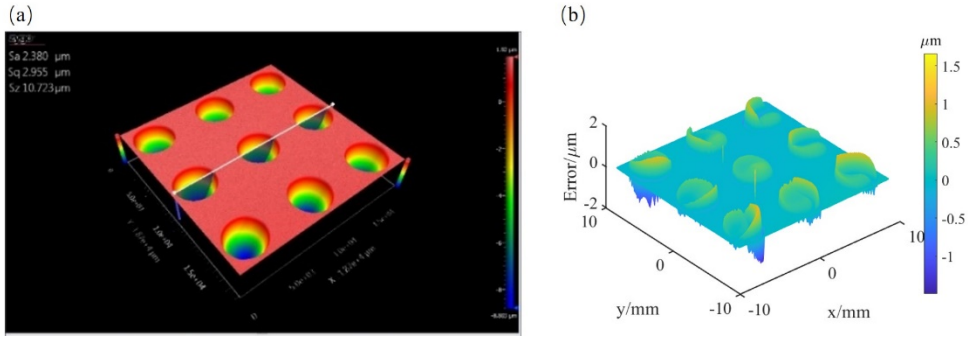

Fig. 8. (a) Machined surface measured using a white light interferometer (10×) and (b) 3D error map for the measured MLAs.

RMS and *PV* values are 0.19 μm and 3.15 μm, respectively.

$$RMS = \sqrt{\frac{1}{N}\sum_{i=1}^{N} z_i^2(x,y)}$$
$$PV = \left| \max_N(z_i(x,y)) \right| + \left| \min_N(z_i(x,y)) \right| \tag{8}$$

where $z_i(x,y)$ are the z values for the surface, with the calculation of a total of N points. The machined errors were mainly found to be distributed in locations with a large surface curvature. It is noted that lenses that are farther from the central lens exhibit a poorer surface quality, and errors around the boundary region of each lens are significantly higher than those in the central region. The reason for this can be attributed to the volumetric positioning errors and dynamic errors in the machining process. Moreover, the form accuracy is sensitive to the introduction of re-clamping errors, which can lead to a failure to improve the surface quality.

3.3. Micro-abrasive fluid jet polishing

The polishing experiments were conducted using a ZEEKO IRP200 polishing machine, as shown in Fig. 4. The compensation polishing process not only needs to correct the holistic errors for the surface but also needs to improve the quality of each lens. The same machining parameters were used, as shown in Table 4.

Table 4. Polishing parameters used in the compensation process

Parameters	Values
Standard-off distance (mm)	8
Pressure (Bar)	8
Feed rate (mm/min)	10
Spacing (mm)	0.1

Figure 9(a) and Fig. 9(b) show the polished workpiece after the compensation process and the 3D error map of the MLA surface. To better analyze the corrected lens quality, the nine lenses were classified into three groups: Central (No. 5), Far (No. 1/3/7/9) and Near (No. 2/4/6/8). As shown in Fig. 9(b), the surface form errors are sharply reduced and range from -0.33 μm to 0.44 μm. The *PV* and *RMS* values for the holistic surface are 0.77 μm and 0.11 μm, respectively.

Figure 10(a) and Fig. 10(b) show the form error for the nine lenses before and after MAFJP. The narrow bars denote the results obtained after polishing, and the wider bars represent the

Optics EXPRESS

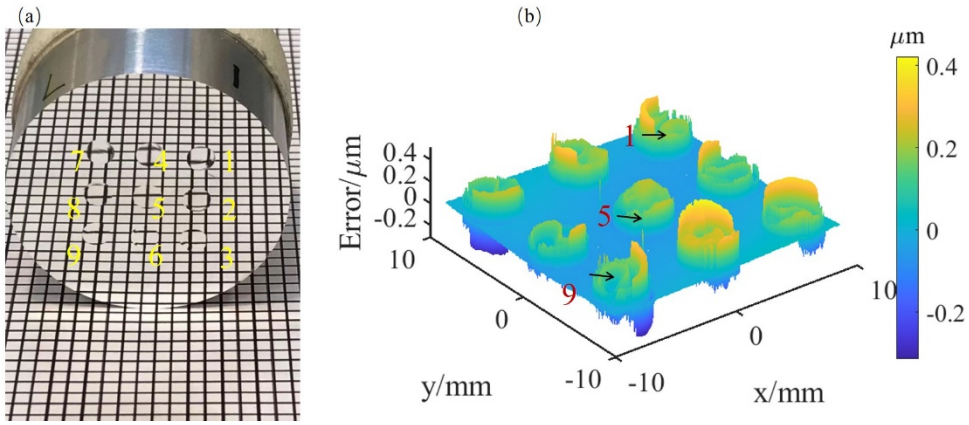

Fig. 9. (a) Polished MLA (b) 3D error map obtained after the polishing process.

results obtained before polishing. From the bar figure, the central lens (No. 5) shows a better surface quality than that for lenses located at far and near positions before the polishing process, but the surface form errors are almost at the same level in terms of the *PV* and *RMS* values after the polishing process. The surface error evaluated for the lenses in terms of the *PV* value is approximately 0.56 μm, while that for the *RMS* value is approximately 0.13 μm.

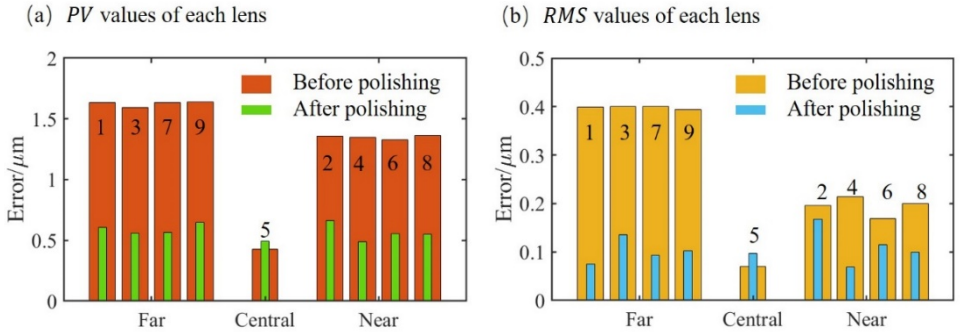

Fig. 10. Comparing the results obtained for the surface errors of the nine lenses in terms of the *PV* and *RMS* values.

In addition, the surface profile extracted for lens 1, including information for the ideal surface before and after polishing the surface, is also compared in Fig. 11. The final deviation at each section is also shown, and the results demonstrate that the corrected lens fits well with the designed lens.

Optics EXPRESS

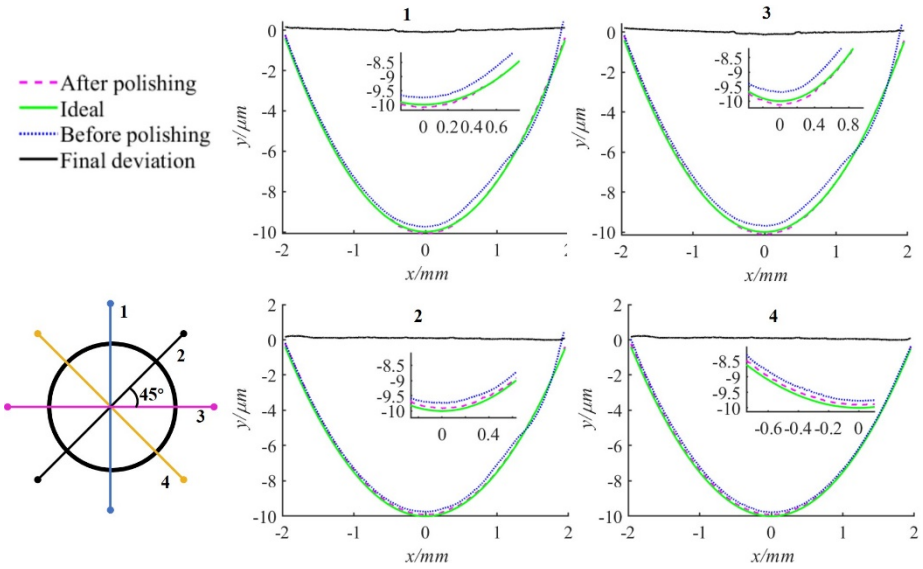

Fig. 11. The surface profiles for lens 1 at four radial sections and four types of profiles are compared, including the ideal, before and after polishing section lines as well as the final deviation between the ideal section profile and that obtained after polishing (local details with larger magnification were also shown).

4. Discussion

From the obtained surface error by using ultra-precision turning and a micro-abrasive fluid jet polishing process chain, it is clear that the added MAFJP can achieve a better surface accuracy. A significant improvement in the *PV* value of 65% (from 1.67 μm to 0.58 μm) is observed for the lens at the far position and 63% (from 1.46 μm to 0.54 μm) for that at the near position. Moreover, the *RMS* value for the lenses at the far position is decreased from 0.4 μm to 0.1 μm, and that value at the near position is also decreased by an average of more than 50% to 0.1 μm on average. Compared with the results obtained before the polishing process, a smoother and more uniform surface quality with a smaller surface form error of 0.56 μm is achieved by MAFJP for the nine lenses. It is interesting to note that the combined process chain has relatively little influence on the surface quality of the lens located at the central zone of the workpiece. This is because the compensation process with MAFJP under the conditions of the polishing parameters and strategy used has limited capacity to smooth the freeform surface and can improve the surface accuracy down to a *PV* value of approximately 0.54 μm.In this experimental research, the form errors obtained for the MLAs are larger than that obtained for the simulated results for the flat surface with *PV* values of 0.4 μm and 0.56 μm, respectively. This deviation can be caused by the uncertainty in the fitted model, which can be used to compensate for the different degrees of material removal when the impingement angle and surface curvature change in the real polishing process.

5. Conclusion

In this paper, a two-cycle machining process chain method that combines diamond turning with micro-abrasive fluid jet polishing (MAFJP) process to improve the surface quality of MLA was developed. An ultra-precision diamond machining process chain was first used to machine a MLA with the maximum possible surface form accuracy. After that, a positioning method was explored to transfer the form error to the polishing system, and then the polishing method with

Optics EXPRESS

optimized polishing conditions was applied to further improve the surface quality and reduce the nonuniformity error for each lens. Both simulations and experimental studies were carried out to demonstrate the reliability of our proposed method, which overcomes the limitations of existing diamond machining technologies in terms of the avoidance of nonuniformity and improvement of the form accuracy in the manufacturing of microlens arrays. The main conclusions are highlighted as follows:

1. Although the employed SPDT process chain can achieve a surface accuracy in terms of *PV* and *RMS* values that reach as high as 1.67 µm and 0.198 µm, respectively, the combined MAFJP process is not only capable of improving the surface accuracy by more than 50% but also of reducing the nonuniformity of each lens to a *PV* value of 0.56 µm.

2. The employment of two-step tool path generation and the fitted model for the compensation error of the freeform surface via MAFJP can lead to a great improvement in surface quality.

Funding. Science and Technology Commission of Shanghai Municipality (21PJ1401100); Research Grants Council of the Government of the Hong Kong Special Administrative Region (15200119); Fudan University-CIOMP Joint Fund (FC2020-006).

Disclosures. The authors declare no conflicts of interest.

Data availability. Data underlying the results presented in this paper are not publicly available at this time but may be obtained from the authors upon reasonable request.

References

1. S.-I. Chang, J.-B. Yoon, H. Kim, J.-J. Kim, B.-K. Lee, and D. H. Shin, "Microlens array diffuser for a light-emitting diode backlight system," Opt. Lett. **31**(20), 3016–3018 (2006).
2. L. Kong and P. Zhou, "A light field measurement system through PSF estimation by a morphology-based method," Int. J. Extrem. Manuf. **3**(4), 045201 (2021).
3. M. S. Uddin, K. Seah, M. Rahman, X. Li, and K. Liu, "Performance of single crystal diamond tools in ductile mode cutting of silicon," J. Mater. Process. Technol. **185**(1-3), 24–30 (2007).
4. X.-W. Cao, Q.-D. Chen, L. Zhang, Z.-N. Tian, Q.-K. Li, L. Wang, S. Juodkazis, and H.-B. Sun, "Single-pulse writing of a concave microlens array," Opt. Lett. **43**(4), 831–834 (2018).
5. G. Cusanelli, A. Hessler-Wyser, F. Bobard, R. Demellayer, R. Perez, and R. Flükiger, "Microstructure at submicron scale of the white layer produced by EDM technique," J. Mater. Process. Technol. **149**(1-3), 289–295 (2004).
6. S. Tanikawa and J. Yan, "Fabrication of micro-structured surface with controllable randomness by using FTS-based diamond turning," Precis. Eng. **73**, 363–376 (2022).
7. S. Wang, C. Cheung, M. Ren, and M. Liu, "Fiducial-aided on-machine positioning method for precision manufacturing of optical freeform surfaces," Opt. Express **26**(15), 18928–18943 (2018).
8. K. Nagayama and J. Yan, "Deterministic error compensation for slow tool servo-driven diamond turning of freeform surface with nanometric form accuracy," Journal of Manufacturing Processes **64**, 45–57 (2021).
9. W. Yuan, L.-H. Li, W.-B. Lee, and C.-Y. Chan, "Fabrication of microlens array and its application: a review," Chin. J. Mech. Eng. **31**(1), 16 (2018).
10. D. Li, B. Wang, Z. Qiao, and X. Jiang, "Ultraprecision machining of microlens arrays with integrated on-machine surface metrology," Opt. Express **27**(1), 212–224 (2019).
11. M. Mukaida and J. Yan, "Fabrication of hexagonal microlens arrays on single-crystal silicon using the tool-servo driven segment turning method," Micromachines **8**(11), 323 (2017).
12. L. Zhang, N. J. Naples, W. Zhou, and Y. Y. Allen, "Fabrication of infrared hexagonal microlens array by novel diamond turning method and precision glass molding," J. Micromech. Microeng. **29**(6), 065004 (2019).
13. Z. Sun, S. To, S. Wang, and J. Du, "Development of self-tuned diamond milling system for fabricating infrared micro-optics arrays with enhanced surface uniformity and machining efficiency," Opt. Express **28**(2), 2221–2237 (2020).
14. Y. B. Kim, J. Park, W. S. Lee, and J. K. Lee, "Fabrication of microlens array by the tilted milling method to improve the surface morphology," Mater. Manuf. Processes **36**(10), 1171–1177 (2021).
15. A. Beaucamp, Y. Namba, and R. Freeman, "Dynamic multiphase modeling and optimization of fluid jet polishing process," CIRP Ann. **61**(1), 315–318 (2012).
16. S. Wan, X. Zhang, H. Zhang, M. Xu, and X. Jiang, "Modeling and analysis of sub-aperture tool influence functions for polishing curved surfaces," Precis. Eng. **51**, 415–425 (2018).
17. C. Wang, C. F. Cheung, L. Ho, M. Liu, and W. B. Lee, "A novel multi-jet polishing process and tool for high-efficiency polishing," Int. J. Mach. Tools Manuf. **115**, 60–73 (2017).
18. C. Wang, Z. Zhang, C. F. Cheung, W. Luo, Y. M. Loh, Y. Lu, L. Kong, and S. Wang, "Maskless fluid jet polishing of optical structured surfaces," Precis. Eng. **73**, 270–283 (2022).

Optics EXPRESS

19. L. Buss, Y. Qi, J. Heidhoff, O. Riemer, and U. Fritsching, "Towards an understanding of multiphase fluid dynamics of a microfluid jet polishing process: a numerical analysis," Fluids **7**(3), 119 (2022).
20. F. R. Menter, "Two-equation eddy-viscosity turbulence models for engineering applications," AIAA J. **32**(8), 1598–1605 (1994).
21. H. Qi, Z. Xie, T. Hong, Y.-y. Wang, F.-z. Kong, and D.-h. Wen, "CFD modelling of a novel hydrodynamic suspension polishing process for ultra-smooth surface with low residual stress," Powder Technol. **317**, 320–328 (2017).
22. C. Wang, C. F. Cheung, and M. Liu, "Numerical modeling and experimentation of three dimensional material removal characteristics in fluid jet polishing," Int. J. Mech. Sci. **133**, 568–577 (2017).
23. T. Wang, H. Cheng, Y. Chen, and H. Tam, "Multiplex path for magnetorheological jet polishing with vertical impinging," Appl. Opt. **53**(10), 2012–2019 (2014).
24. C. F. Cheung, C. Wang, L. T. Ho, and J. Chen, "Curvature-adaptive multi-jet polishing of freeform surfaces," CIRP Ann. **67**(1), 357–360 (2018).
25. H.-y. Tam and H. Cheng, "An investigation of the effects of the tool path on the removal of material in polishing," J. Mater. Process. Technol. **210**(5), 807–818 (2010).
26. A. Beaucamp, K. Takizawa, Y. Han, and W. Zhu, "Reduction of mid-spatial frequency errors on aspheric and freeform optics by circular-random path polishing," Opt. Express **29**(19), 29802–29812 (2021).
27. Z.-C. Cao, C. F. Cheung, and M. Ren, "Modelling and characterization of surface generation in fluid jet polishing," Precis. Eng. **43**, 406–417 (2016).
28. S. Wan, X. Zhang, M. Xu, W. Wang, and X. Jiang, "Region-adaptive path planning for precision optical polishing with industrial robots," Opt. Express **26**(18), 23782–23795 (2018).
29. X. Zhang, H. Zhang, X. He, M. Xu, and X. Jiang, "Chebyshev fitting of complex surfaces for precision metrology," Measurement **46**(9), 3720–3724 (2013).
30. M. Greenspan and G. Godin, "A nearest neighbor method for efficient ICP," in *Proceedings Third International Conference on 3-D Digital Imaging and Modeling*, (IEEE, 2001), 161–168.